Decision making in noisy bistable systems with time-dependent asymmetry

Nuno R. Nené[1] and Alexey Zaikin[2]
[1]*Department of Mathematics, Imperial College London, South Kensington Campus, SW7 2AZ London, United Kingdom*
[2]*Institute for Women's Health and Department of Mathematics, University College London, Gower Street, WC1E 6BT London, United Kingdom*

(Received 9 July 2012; revised manuscript received 3 December 2012; published 22 January 2013)

Our work draws special attention to the importance of the effects of time-dependent parameters on decision making in bistable systems. Here, we extend previous studies of the mechanism known as speed-dependent cellular decision making in genetic circuits by performing an analytical treatment of the canonical supercritical pitchfork bifurcation problem with an additional time-dependent asymmetry and control parameter. This model has an analogous behavior to the genetic switch. In the presence of transient asymmetries and fluctuations, slow passage through the critical region in both systems increases substantially the probability of specific decision outcomes. We also study the relevance for attractor selection of reaching maximum values for the external asymmetry before and after the critical region. Overall, maximum asymmetries should be reached at an instant where the position of the critical point allows for compensation of the detrimental effects of noise in retaining memory of the transient asymmetries.

DOI: 10.1103/PhysRevE.87.012715 PACS number(s): 87.18.Cf, 05.45.−a, 87.18.Tt

I. INTRODUCTION

The problem of cell fate decision has been recently equated with gene expression pattern selection [1] as a response to a combination of external signals. These data sets have been invaluable in corroborating the hypothesis that cue signals that induce distinct cell phenotypes, e.g., in differentiation, can to an extent be associated with mutually exclusive expression stable programs or high-dimensional attractors in an epigenetic landscape. The integration of cue signals is initially performed by the signaling system, whose function is akin to a multilayer perceptron [2]. The outcome of this signal processing step is a combination of activation concentration profiles of the output nodes, normally kinase proteins, whose amplitude and duration have been correlated with the induced genetic programs [3,4]. The transcriptional machinery subsequently integrates a wealth of input signal combinations, which may induce bifurcations in the system's behavior and consequently affect cellular decision making [5]. Signals not only drive transcriptional landscape changes but also create the appropriate asymmetries, enhancing the probability of reaching the attractors that encode the adequate evolutionary response. The question arises as to what extent are the combinations associated with only one attractor, and which signal characteristics are important in attractor selection in the face of fluctuations.

One particular signal characteristic that has just recently been explored is the rising time of external signals [6,7]. The time-dependent profile of external signals may induce significant effects near bifurcation points when fluctuations are considered. In fact, the theory presented here relates back to the mechanism for cell fate decision known as speed-dependent cellular decision making (SdCDM) observed in low order circuit models [6].

In [6], it was shown that the combination of external signals is most efficient in selecting a specific attractor, in the face of fluctuations, when the rising times are larger. This is a consequence of larger rising times corresponding to smaller sweeping speeds through the critical region and consequently to smaller switching delays [8]. To further clarify aspects behind speed-dependent mechanisms, we will resort here to the bistable potential problem arising from the normal form for a supercritical pitchfork bifurcation affected by an external field [see Eq. (1) and Figs. 1(a) and 1(b)]. This one-dimensional problem allows for analytical treatment and is qualitatively equivalent, with respect to rate-dependent effects in the presence of fluctuations, to the decision genetic switch explored before [6], when the bifurcation parameter and external asymmetry, $\lambda(t)$ and $g(t)$, respectively [see Eq. (1)], are made time dependent. In these circumstances, both systems are forced through a bifurcation in the presence of a transient external asymmetry, here imposed by $g(t)$, and, in [6], arising from the combination of external signals driving the genetic circuit. We will also analyze the consequences of reaching the maximum asymmetry before, at, and after $\lambda_c = 0$, which is the original bifurcation point when $g(t) = 0$ [Fig. 1(a)]. This will further the study performed in genetic networks and possibly help to understand aspects inherent to the analytical reduction of the original gene regulatory network model [6] to standard normal forms [9] such as that studied in this work [see Eq. (1)]. The pitchfork bifurcation, in its super- or subcritical form, has been seen as the standard model in genetic circuits behind, for example, decision making in haematopoietic cell differentiation regulated by the GATA1 and PU.1 master regulators [5,10]. Yet, this regulatory system can also show other valid bifurcation types, e.g., saddle-node bifurcation [11], depending on the combination of external signals driving it. Our choice of a pitchfork bifurcation allows us to link our findings to previous theoretical work on dynamic bifurcations and serves as a stepping stone to future investigations of speed-dependent effects in noisy genetic networks, where several types of transitions may occur due to the coexistence of several distinct dynamical regimes [12].

The paper is structured as follows. In Sec. II, we explore in a deterministic scenario the effects on the trajectories of considering several time-dependent asymmetry functions and several sweeping rates. In Sec. III, we test the results obtained in Sec. II against the detrimental effects of fluctuations, both by extensive numerical simulations and analytical solutions

for the probability of reaching a specific attractor during the sweeping process.

II. SWITCHING DYNAMICS IN THE BISTABLE POTENTIAL PROBLEM WITH TIME-DEPENDENT PARAMETERS

Let us first analyze Eq. (1) with constant parameters. In the case of the external asymmetry being zero, $g(t) = 0$, Eq. (1) admits for $\lambda < 0$ the unique asymptotically stable solution $X = 0$. For $\lambda > 0$, three solutions appear: the asymptotically stable branches given by $\pm\sqrt{X}$ and the trivial unstable solution $X = 0$ [see Fig. 1(a)],

$$\dot{X} = \lambda(t)X - X^3 + g(t). \tag{1}$$

In a situation when $g(t) = g = \text{const} > 0$, the bifurcation point previously observed [see Fig. 1(a)] disappears giving place to a connected set of solutions with positive values, X_+, a disconnected branch with negative values, X_- [see Fig. 1(b)], and an unstable branch X_u. One should add that the connected and disconnected branches swap their positions if the asymmetry is <0. Yet, all of the properties observed for $g(t) > 0$ are maintained when $g(t) < 0$. Regarding λ_i [see Fig. 1(b)], the point where the three solutions appear, it is displaced from the original bifurcation point $\lambda_c = 0$ by a distance given by $\lambda_i - \lambda_c = 3(\frac{g}{2})^{\frac{2}{3}}$. Therefore, the minimum distance between the two branches is given by $d_{\min} = (\Delta X)_{\lambda=\lambda_i} = (X_+ - X_-)_{\lambda=\lambda_i} = 3(\frac{g}{2})^{\frac{1}{3}}$ [see also Fig. 1(b)]. The previous expression can be found by computing the point where the three solutions appear. This can be estimated by recurring to the discriminant (Δ) of the cubic equation, $-X^3 + \lambda X + g$, and finding the roots satisfying $\Delta = 4\lambda^3 - 27g = 0$. When the discriminant is zero, there is a double real root, which is the situation of interest for the problem in hand. Regarding the unstable branch of solutions, its position far below or above $\lambda = 0$ can be estimated to be displaced approximately by $-\frac{g}{\lambda - \lambda_c}$ when $g(t) = g = \text{const}$.

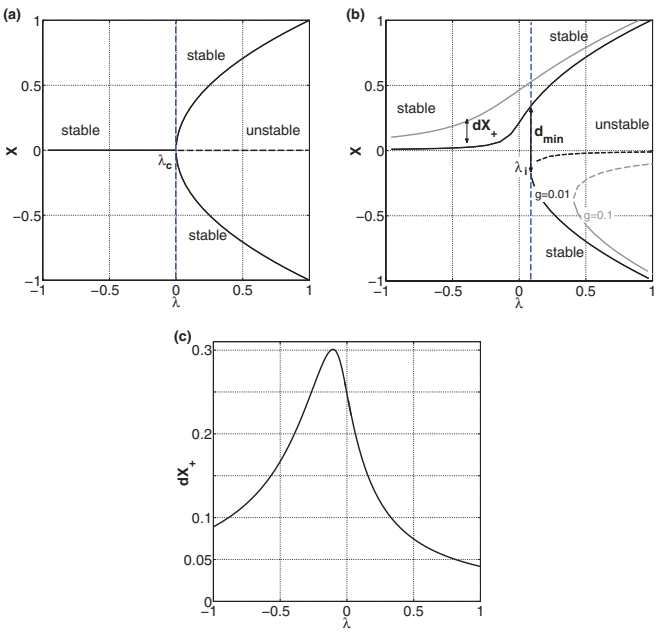

FIG. 1. (Color online) Comparative bifurcation diagrams for different parameters of a supercritical pitchfork bifurcation normal form, symmetric, and asymmetric. (a) $g(t) = 0$. (b) $g(t) = 0.01$ and $g(t) = 0.1$ [Eq. (1)]. The presence of a constant external asymmetry induces a disconnection of the solution branches. $d_{\min}$ represents the minimum distance between positive and negative branches, $d_{\min} = (\Delta X)_{\lambda=\lambda_i} = (X_+ - X_-)_{\lambda=\lambda_i}$. (c) Distance $dX_+ = (X_+)_{g(t)=0.1} - (X_+)_{g(t)=0.01}$, between the upper branch of solutions of a supercritical pitchfork bifurcation for constant $g(t) = 0.1$ and $g(t) = 0.01$ [see (b)]. The major differences in dX_+ arise near the original bifurcation point of Eq. (1) with $g(t) = 0$ [see also (a)]. After $\lambda = 0$, the major differences in the bifurcation diagrams arise in the position of λ_i and in the sizes of basins of attraction [see (b)]. The bifurcation diagrams represented in (a) and (b) were generated in XPPAUT by finding the steady-state solutions of Eq. (1) with the available continuation methods [13].

The effect of the asymmetry as a state selector when the system is swept through the critical region, for $|g(t)| \ll 1$, is expected to be more pronounced near the bifurcation point due to the disconnection between branches [see Fig. 1(b)]. The sensitivity to different asymmetry amplitudes is also expected to be more pronounced near the critical point due to differences in the inflexion of the connected branch [observe the profile for dX_+ in Fig. 1(c)] and the position of λ_i [see Fig. 1(b)]. A constant external asymmetry plus noise has been demonstrated to induce a higher selectivity, equated with the ratio between the number of trajectories reaching the branch favored by g and the total simulated trajectories, when the bifurcation parameter λ is varied in time with lower speeds [8,14]. This occurs due to the fact that in these circumstances, switching delays are less pronounced. This finding has relevance to the problem of cell fate decision and has been also demonstrated in genetic circuits [6].

In the work presented here, we extend the findings of speed-dependent effects near bifurcation points [8] to include a transient external asymmetry $g(t)$. This particular study has not been performed before and is important to understand the system's memory of external signals.

Determining numerically the deterministic sample paths of a system ruled by Eq. (1), we can show the effects of varying in time both the asymmetry g and the critical parameter λ. The system is initially started at $X = 0$, which for $-1 < \lambda < 0$ is the only solution of Eq. (1). The critical parameter is subsequently changed according to a linear law, $\lambda(t) = \lambda_0 + \gamma_\lambda t$, from $\lambda_0 = -1$ to $\lambda_F = 1$, with sweeping speed γ_λ, after which it is maintained at λ_F. The asymmetry, on the other hand, follows a piecewise linear law [see Fig. 2(a) and Eq. (2)]:

$$g(t) = \begin{cases} \gamma_{g_1} t & \text{if} \quad 0 \leqslant t \leqslant T_{g_1}, \\ g_{\max} - \gamma_{g_2}(t - T_{g_1}) & \text{if} \quad T_{g_1} \leqslant t \leqslant T_\lambda, \\ 0 & \text{if} \quad t \geqslant T_\lambda. \end{cases} \tag{2}$$

Three cases were explored: the maximum external asymmetry $g_{\max}$ being reached at the precise instance $t = T_{\lambda=0}$ when the critical parameter λ reaches 0 [the original bifurcation point for $g(t) = 0$; see Fig. 1(a)], and just before ($t = T_{g_1} = \frac{T_\lambda}{4} < T_{\lambda=0}$) or after ($t = T_{g_1} = \frac{3T_\lambda}{4} > T_{\lambda=0}$) [see also Fig. 2(a)]. We impose, therefore, a dependence of the rates γ_{g_1} and γ_{g_2} on γ_λ. We should emphasize that the functions for both $\lambda(t)$ and $g(t)$ are motivated by the previous study of nonequilibrium gene regulatory network models performed in [6]. Typically,

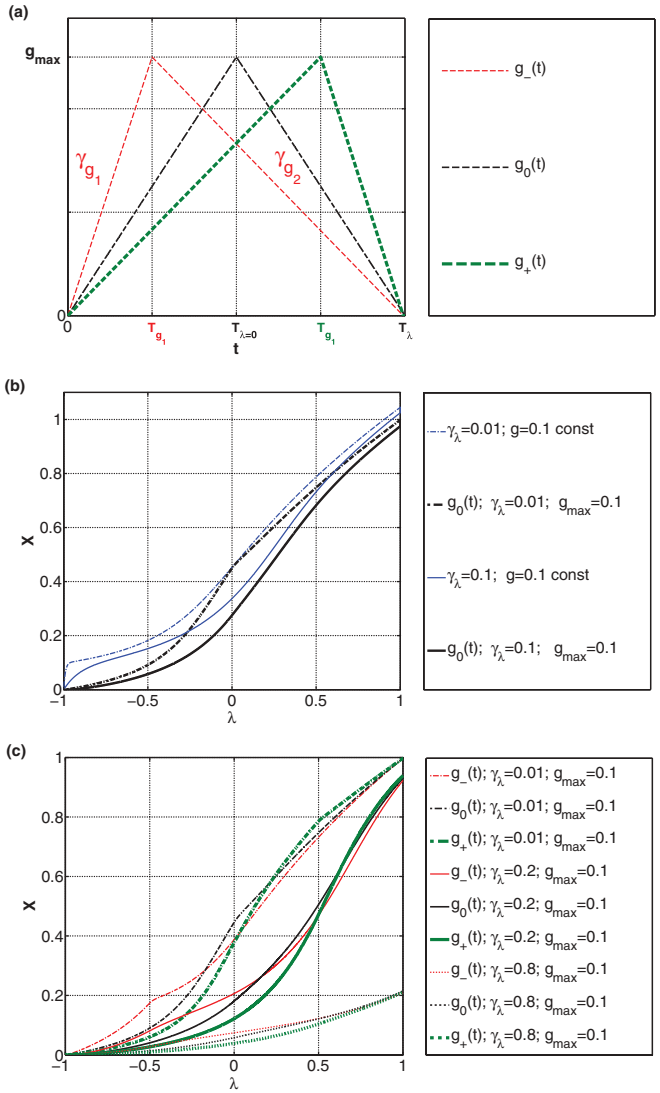

FIG. 2. (Color online) Effects of time-dependent critical parameter and asymmetry on the deterministic trajectories of X. (a) Profile for $g_{-}(t)$ with $T_{g_1} = \frac{T_\lambda}{4}$, $g_0(t)$ with $T_{\lambda=0} = \frac{T_\lambda}{2}$, and $g_{+}(t)$ with $T_{g_1} = \frac{3T_\lambda}{4}$ [see also Eq. (2)]. γ_{g_1} and $-\gamma_{g_2}$ are given by $\frac{g_{\max}}{(T_{g_1})}$ and $\frac{-g_{\max}}{(T_\lambda - T_{g_1})}$, respectively. $g_{\max}$ stands for maximum asymmetry of $g_{0,\pm}(t)$. (b) X vs λ for sweeping speed $\gamma_\lambda = 0.01$ and 0.1 and time-dependent asymmetry $g_0(t)$ [see (a)] with $g_{\max} = 0.1$. Also shown is the trajectory for constant asymmetry $g(t) = 0.1$. (c) X profile for $\gamma_\lambda = 0.01$, 0.2, and 0.8 and time-dependent asymmetry $g_{-}(t)$ (with $T_{g_1} = \frac{T_\lambda}{4}$), $g_0(t)$ (with $T_{g_1} = T_{\lambda=0} = \frac{T_\lambda}{2}$), and $g_{+}(t)$ (with $T_{g_1} = \frac{3T_\lambda}{4}$), for $g_{\max} = 0.1$ [see (a)]. In (c), the differences in the positions of the trajectories at $\lambda = 1$ stem from the delayed switching when larger sweeping rates γ_λ are considered. After $\lambda = 1$, the plots should converge vertically to the steady-state solution. In (b), the same observation holds with the exception of the differences between the blue and black curves, which stem from the imposed different asymmetry functions.

external signals have complex profiles [15] and specificity to each of the signal characteristics has been proven to occur, to an extent, in the gene expression patterns induced [3,4]. However, here we focus on the effects of sweeping the system through its bifurcation region in one direction, therefore simplifying the analytical problem. Consequently, the choice of linear and piecewise linear functions for $\lambda(t)$ and $g(t)$, respectively, represent simply the effects of external signals with only rising times and saturating at an equal level [6]. Further studies where a combination of ramplike and oscillatory signals drive the system through the bifurcation point should reveal the links between phenomena akin to stochastic resonance [16] and cell fate decision in genetic networks where coexistence of complex signals is the norm.

Observing the results presented in Fig. 2(b), we notice that switching from $X = 0$ with $g(t) = \text{const}$ occurs at later values of λ if the speed of parameter driving is increased. The instant where the jump occurs can be demonstrated to be proportional to $1/\gamma_\lambda$ [17,18]. The switching point is further increased if we apply $g_0(t)$ [Fig. 2(b); observe the differences in the profiles of blue and black lines]. Together with higher switching delays, the potential minima of the cases where the asymmetry is time dependent are dislocated to lower values of X [observe the differences at $\lambda = 1$; Fig. 2(b)]. This stems from the fact that the asymmetry returns to zero.

Regarding the effects on the sample paths of $g_{\pm}(t)$ with respect to $g_0(t)$, Fig. 2(c) shows us that the position of the trajectories is regulated by the order of the instants where the maximum of each of the functions is achieved. Yet, the differences between paths become smaller at larger times [due to saturation effects exerted by the cubic term in Eq. (1); see also Fig. 1(c)]. This will be an important point when fluctuations are considered further ahead. Additionally, if the sweeping speed γ_λ is increased, the differences between the trajectories obtained by applying each of the asymmetry profiles $g_{0,\pm}(t)$ is reduced [compare in Fig. 2(c) the interrupted line and full line plots].

III. DECISION MAKING IN THE PRESENCE OF FLUCTUATIONS

If noise is included, how will the selectivity of each of the attractor branches be affected by both the speed γ_λ of parameter driving and the maximum asymmetry $g_{\max}$? Sample trajectories for a small asymmetry $g_{\max} = 0.1$ and noise intensity $\sigma = 0.05$ are represented in Fig. 4(b). Both the cases of time-dependent $g_0(t)$ [see Fig. 2(a)] and constant asymmetry are plotted. We used the Langevin equation associated with Eq. (1) by adding a Gaussian distributed noise term $\xi_{X,Y}(t)$, i.e., with zero mean and correlation $\langle \xi_X(t), \xi_Y(t') \rangle = \sigma^2 \delta_{XY} \delta(t - t')$. All of the numerical results presented throughout this paper were performed by resorting to a Heun method [19].

It is possible to check that the trajectory with additional time-dependent asymmetry has, as was seen for the deterministic case [Fig. 2(b)], a path closer to the unstable branch of solutions of the bifurcation diagram. This may enhance the probability of jumping across the potential barrier that coincides with the unstable branch. For higher intensities of noise, the role of the asymmetry $g(t)$ as a state selector may be decreased. The trajectories may be capable of crossing to the lower branch even when the critical parameter has reached a considerable value with which a sufficient depth of the potential is achieved. The transition dynamics time scale between minima can be estimated using Kramers classical

theory [20] and its improvements [17]. Overall, the critical parameter has to be swept with a sufficiently low speed to induce the maximum probability of the system migrating to the branch of solutions favored by $g(t)$. Yet, the speed has to be sufficiently high to increase the potential barrier and as a result increase the transition time to the lower branch [17]. If these conditions are met, we reduce the probability of a jump erasing the effect of the transient external signal.

Let us devise analytical expressions in order to quantify thoroughly the effects of noise and sweeping speed γ_λ on attractor selectivity when the external asymmetry is made time dependent and, thus, predict the number of trajectories that reach a specific branch. For the analytical treatment, we will resort to the Fokker-Planck equation associated with the respective Langevin equation of Eq. (1). Several assumptions underlie the applicability of the following theoretical approach [8]. First, the distribution around the branch of solutions before the critical point is assumed to be Gaussian. As the control parameter λ is passed through the critical region, the distribution starts to drift towards the branch favored by $g(t)$. The drift rate is approximately $g(t)$. In this region, the relaxation to the equilibrium is slow. At $\lambda = 0$, the position of the steady state is approximately $[g(t = T_{\lambda=0})]^{1/3}$, which makes the relaxation time $[g(t = T_{\lambda=0})]^{-2/3}$. For very small asymmetries, this relaxation process is extremely slow [21]. Concurrently with the drift process, the distribution also suffers spreading due to the fluctuations represented by the noise term shown above. Around the critical region, the amplitude of the fluctuations is amplified [18]. Nevertheless, if a strong external field $g(t)$ is applied, the effects of the fluctuations can be neglected if the critical parameter λ is slowly changed. Sweeping with large enough rates allocates a larger importance to the presence of fluctuations, which may determine to a large extent the equilibrium state selected [18]. After the critical point, the distribution becomes bimodal with each peak centered on the respective stable branch, X_+ or X_-. A second assumption lies with the fact that a Gaussian-like distribution for the process is only valid if the speed with which the critical parameter is forced to go through the critical region is sufficiently high. If this condition is not met, then the distribution relaxes to its non-Gaussian form and the analytical solutions determined in the following section are not sufficiently descriptive [8,22]. It is expected that an optimum selection process occurs if the critical parameter is changed with a speed that allows for the drift to center the distribution on a point that shifts most of the area under the curve beyond the position of the unstable branch at approximately $T_{\lambda=0}$. Unlike studies devising analytical approaches based on attractor to attractor transition theory for the probability density mass transfer across the potential barrier [16,17], we will assume, for the sake of simplicity, that the attractor selection process is complete just after the bifurcation point [8].

We also must stress that our approach does not address the concept of stochastic bifurcations [23]. Our work is based on the currently accepted assumption that the switching dynamics explored in Sec. II occurs due to the appearance of the bifurcation point even in the presence of fluctuations. Moreover, we will only focus on small maximum asymmetries $g_{\max}$. For much larger external asymmetries, the switching dynamics will be less pronounced due to the gap between branches and, therefore, the reduced differences between the connected branch before and after the critical point. In the next sections, we will draw special attention only to the possibility of even relatively small asymmetries being discriminated in the face of fluctuations when the sweeping speed γ_λ is small enough.

A. Attractor selection depends on the maximum of the transient asymmetry to noise ratio and the critical parameter sweeping speed

The probability density function $P(X,t)$ can be described by Eq. (3) derived for the Langevin equation of the bistable potential represented in Eq. (1) [20],

$$\frac{\partial P(X,t)}{\partial t} = -\frac{\partial}{\partial X}\{[\lambda(t)X - X^3 + g(t)]P(X,t)\} + \frac{\sigma^2}{2}\frac{\partial^2 P(X,t)}{\partial X^2}. \tag{3}$$

Here we do not take into account any fluctuations in the set of parameters. Their contribution is thought to be negligible for the calculations to follow [8]. The evolution of the probability density function $P(X,t)$ can be calculated by finding how each of the distribution moments changes during the sweeping process. By multiplying Eq. (3) by X^n, neglecting the cubic term (near the bifurcation point, where the selection process is assumed to occur, $X \ll 1$), and integrating by parts, one obtains an expression which can lead to an equation for each of the moments of the probability density function. Assuming that the first two moments are sufficiently descriptive of the evolution of the probability density function $P(X,t)$ near the bifurcation point, we chose to restrict our analysis to Eq. (4) (mean) and Eq. (5) (variance),

$$\frac{d\langle X\rangle}{dt} = \lambda(t)\langle X\rangle + g(t), \tag{4}$$

$$\frac{d\langle(\delta X)^2\rangle}{dt} = 2[\lambda(t)\langle(\delta X)^2\rangle + g(t)\langle X\rangle] + \sigma^2. \tag{5}$$

For a maximum asymmetry $g_{\max} \ll 1$, the contribution of $g(t)$ near the bifurcation point may be assumed to disappear from the equation for the second moment [Eq. (5)]. To an extent, this approximation is always valid for large enough noise intensity and small enough $g_{\max}$ [see Figs. 3(a), 3(c), and 3(d)]. Yet, in certain situations, this may not be so [see Fig. 3(b)]. However, throughout this paper, we will focus on expressions obtained when the simplified version of Eq. (5) is considered and secure that we are in the region where this approximation is justified. In any case, if we consider the $g(t)\langle X\rangle$ term in Eq. (5), then the derivation of expressions for branch selectivity, i.e., number of trajectory reaching X_+, becomes very cumbersome. Therefore, eliminating the contribution of $g(t)$ from the evolution of the variance is necessary for the sake of simplicity.

For our particular problem, and as was stated before, we are interested in the effects of a monotonous linear function for the bifurcation parameter $\lambda(t)$ and for the asymmetry $g(t)$, a piecewise linear function [see Eq. (2)]. Equations (4) and (5) are linear ordinary differential equations and have, therefore, an analytical solution. Through an appropriate change of variables, $t' = \sqrt{\gamma_\lambda(t - \frac{\Delta\lambda}{\gamma_\lambda})}$, with $\Delta\lambda = \lambda_c - \lambda_0$,

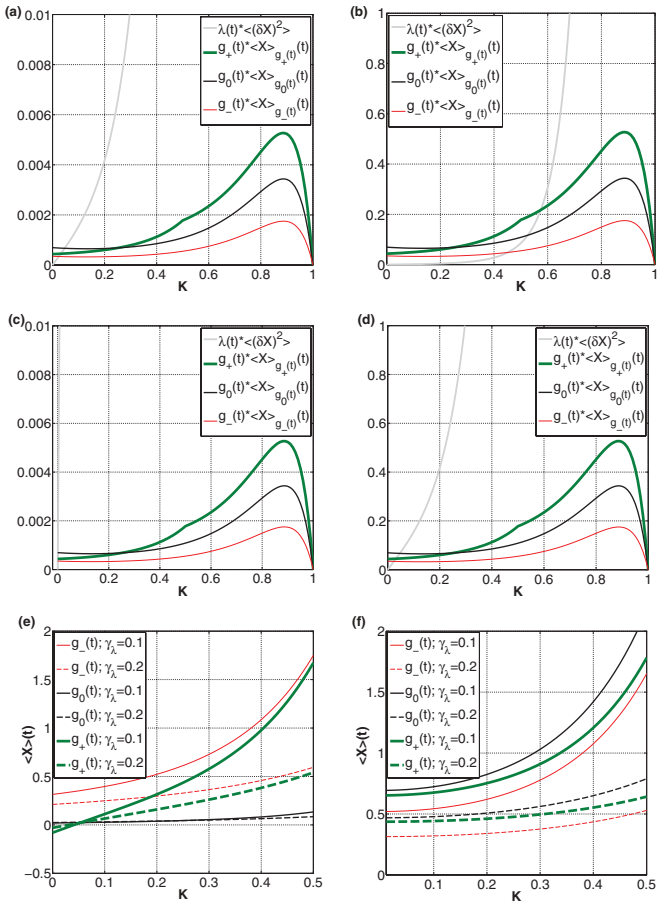

FIG. 3. (Color online) Limits for analytical approximations and profile for the moments describing the sweeping process. Comparison between terms $\lambda(t)\langle(\delta X)^2\rangle$ and $g(t)\langle X\rangle$ in Eq. (5) for each of the external asymmetry profiles $g_{0,\pm}(t)$, with (a) $g_{\max}=0.01$ and $\sigma=0.05$, (b) $g_{\max}=0.1$ and $\sigma=0.05$, (c) $g_{\max}=0.01$ and $\sigma=0.2$, and (d) $g_{\max}=0.1$ and $\sigma=0.2$. (e) First moment calculated through Eq. (10), for $g_{\max}=0.1$, and (f) with the erf(z) function in Eq. (10) approximated to 1, also for $g_{\max}=0.1$.

and assuming that the initial conditions term for each of the expressions is negligible in comparison to the final instance where separation of the initial unimodal distribution is completed, for small enough γ_λ rates we have Eqs. (6) and (9),

$$\langle X\rangle(t)\approx\frac{e^{\frac{(\gamma_\lambda t-\Delta\lambda)^2}{2\gamma_\lambda}}}{\sqrt{\gamma_\lambda}}\left[I_1+I_2\right], \tag{6}$$

$$I_1=\int_{a_1}^{a_2}e^{\frac{-t'^2}{2}}\left[\gamma_{g_1}\left(\frac{t'}{\sqrt{\gamma_\lambda}}+\frac{\Delta\lambda}{\gamma_\lambda}\right)\right]dt', \tag{7}$$

$$I_2=\int_{a_2}^{a_3}e^{\frac{-t'^2}{2}}\left[g_{\max}-\gamma_{g_2}\left(\frac{t'}{\sqrt{\gamma_\lambda}}+\frac{\Delta\lambda}{\gamma_\lambda}-T_{g_1}\right)dt'\right], \tag{8}$$

$$\langle(\delta X)^2\rangle(t)\approx\frac{e^{\frac{(\gamma_\lambda t-\Delta\lambda)^2}{\gamma_\lambda}}}{\sqrt{\gamma_\lambda}}\sigma^2\int_{a_1}^{a_3}e^{-t'^2}dt'. \tag{9}$$

The integration limits in Eq. (7)–(9) are given by $a_1=\frac{(T_{g_1}\gamma_\lambda-\Delta\lambda)}{\sqrt{\gamma_\lambda}}$, $a_2=-\frac{\Delta\lambda}{\sqrt{\gamma_\lambda}}$, and $a_3=\frac{(t\gamma_\lambda-\Delta\lambda)}{(T_{g_1}\gamma_\lambda-\Delta\lambda)}$. Let us study the contribution of $g(t)$ to the mean until an instant t', with $t'\gamma_\lambda=(1+K)\Delta\lambda$ and $K<1$ [8]. This change of variables allows us to eliminate some of the complexity in the expressions devised above. K is simply a measure of how far we are from the bifurcation point in the original case [see Fig. 1(a)], after we have crossed it in the sweeping process. Depending on the proportion of the rates γ_λ, γ_{g_1}, and γ_{g_2}, we will have different cases. By neglecting the term $g(t)\langle X\rangle$ in Eq. (5), the differences arise only in the first moment. For the case of applying $g_0(t)$, where $\gamma_{g_1}=\gamma_{g_2}=g_{\max}\gamma_\lambda$, we have the solution represented in Eq. (10). For the cases of $g_-(t)$ and $g_+(t)$, $\gamma_{g_1}=2g_{\max}\gamma_\lambda$ and $\gamma_{g_2}=\frac{2}{3}g_{\max}\gamma_\lambda$, and $\gamma_{g_1}=\frac{2}{3}g_{\max}\gamma_\lambda$ and $\gamma_{g_2}=2g_{\max}\gamma_\lambda$, respectively. Naturally, similar expressions to Eq. (10) arise by following the same reasoning. We will not present them here explicitly.

The first moment of the distribution generated for each of the external asymmetry functions can be visualized in Figs. 3(e) and 3(f), calculated with the complete expressions [such as Eq. (10)] and with an extra approximation (discussed below), as a function of the distance to $\lambda=0$, measured by K [see Eq. (10)],

$$\langle X\rangle(t)\approx\frac{e^{\frac{K^2}{2\gamma_\lambda}}}{2\gamma_\lambda^{\frac{3}{2}}}g_{\max}[T_1+T_2], \tag{10}$$

$$T_1=2\gamma_\lambda^{\frac{3}{2}}\left(-2+e^{-\frac{1}{2\gamma_\lambda}}+e^{\frac{K^2}{2\gamma_\lambda}}\right), \tag{11}$$

$$T_2=\gamma_\lambda\sqrt{2\pi}\left[\mathrm{erf}\left(\frac{1}{\sqrt{2\gamma_\lambda}}\right)+\mathrm{erf}\left(\frac{K}{\sqrt{2\gamma_\lambda}}\right)\right], \tag{12}$$

$$\langle(\delta X)^2\rangle(t)\approx\frac{e^{\frac{K^2}{\gamma_\lambda}}}{2\sqrt{\gamma_\lambda}}\sigma^2\sqrt{\pi}\left[\mathrm{erf}\left(\frac{1}{\sqrt{\gamma_\lambda}}\right)+\mathrm{erf}\left(\frac{K}{\sqrt{\gamma_\lambda}}\right)\right]. \tag{13}$$

Effectively, by choosing a particular value of K, we are assuming that the selection process is completed when the paths, induced by each of the functions $g_{0,\pm}(t)$, are in a certain order. The results presented in Fig. 3(e) differ from those in Fig. 3(f) due to the fact that in the latter, we assumed that the error function [24] was approximately 1 for small enough sweeping rates. It can be observed that in Fig. 3(e) the order of the moments generated by applying each of the asymmetry profiles is changed with respect to Fig. 3(f). Informed by the numerical results of Figs. 2(b) and 2(c), we would expect that the expressions for the mean without the error function approximated to 1 would generate the correct order for the probabilities of selection of the upper branch X_+. As will be seen ahead, this is not the case. Consequently, since the expression for the variance of each of the external asymmetry profiles is the same [see Eq. (13)], we will resort to the approximated expressions from now on. Another remark should be made about the speed-dependent effects present in the plots for the first moment [see Figs. 3(e) and 3(f)]. As the rate γ_λ is raised, $\langle X\rangle$ stays closer to the unstable branch, both in the curves generated with the approximate and the complete expressions. Additionally, the differences between the moments become smaller with γ_λ in both figures. These observations of speed-dependent switching dynamics are coherent with what was observed in Figs. 2(b) and 3(c). Another important aspect regarding the plots of Figs. 3(e)

and 3(f) is the overall independence of the order of the curves and K. This particular characteristic does not match with the numerical solutions shown in Fig. 2, but is sufficient, nevertheless, to correctly generate the probability curves (discussed ahead). In order to follow with the calculations of the probability of reaching the upper branch of solutions, X_+, we just have to secure that we choose a value of K that justifies the approximation made when the $g(t)\langle X\rangle$ term was neglected from Eq. (5). In addition, K has to be relatively small given the fact that the analytical expressions do not approximate well the steady states for large values. This stems from the elimination of the cubic term from the original normal form equation [see Eq. (1)] when Eqs. (4) and (5) were derived.

Evaluating the selection probability resulting from this sweeping process is, in fact, a way of measuring the memory capacity of the system to transient signals $g(t)$ in the face of fluctuations. For $g_{\max} > 0$, the probability of reaching the favored asymptotic state X_+ is given by integrating the area under the distribution curve that is above $-\frac{g_{\max}}{\lambda_F-\lambda_c}$, which is the estimated position of the asymptotically unstable state, far above or below the critical point, when the asymmetry is constant and equal to $g_{\max}$. This is effectively an overestimate of the actual value for each of the time-dependent asymmetries $g_{0,\pm}(t)$, given that all of them return to zero. Yet, in order to compare the results with those obtained with constant asymmetries [8], we will resort to the mentioned value for the position of the unstable branch. Since the original assumption was that the distribution could be approximated by a Gaussian, in order to calculate the probability P_+ of reaching the upper branch we use the expressions for the mean and variance calculated before [Eqs. (10) and (13)], with the additional approximation of $\mathrm{erf}(z) = 1$ for small enough γ_λ. After an appropriate change of variables, P_+ is given by

$$P_+ = \frac{1}{\sqrt{2\pi}} \int_{-\infty}^{N} e^{-\frac{X'^2}{2}} dX'. \tag{14}$$

In Eq. (14), N stands for the number of standard deviations that the peak of the distribution is displaced from the unstable branch of solutions for a particular value of λ: $N = \frac{[\langle X'\rangle(t')+\frac{g_{\max}}{\lambda_F-\lambda_c}]}{\langle(\delta X)^2\rangle(t)}$. Since $\Delta\lambda = 1$ and $\frac{(K\Delta\lambda)^2}{2\gamma_\lambda} \ll 1$, the second term, $e^{-\frac{(K\Delta\lambda)^2}{2\gamma_\lambda}} \frac{g_{\max}}{\lambda_F-\lambda_c}$, in the numerator of the full expression for N can be neglected for small enough sweeping rates. The expression for the probability P_+ of attractor selection can thus be computed [see Eq. (15)]. For sweeping rates γ_λ bigger than 1, we can also simplify the P_+ calculation by performing asymptotic expansion of the error functions and retaining only the first term. This will not be done here.

$$\begin{aligned} P_+ &= \frac{1}{2}\left(1+\mathrm{erf}\left\{\alpha\frac{g_{\max}}{\sigma}\left[F_{g_{0,\pm}(t)}\left(\frac{\gamma_\lambda}{\pi}\right)^{\frac{1}{4}}+\beta\left(\frac{\pi}{\gamma_\lambda}\right)^{\frac{1}{4}}\right]\right\}\right), \\ &\leqslant \frac{1}{2}\left\{1+\mathrm{erf}\left[\frac{g_{\max}}{\sigma}\left(\frac{\pi}{\gamma_\lambda}\right)^{\frac{1}{4}}\right]\right\}. \end{aligned} \tag{15}$$

In Eq. (15), for the case of $g_0(t)$ [see Fig. 2(a)], $F_{g_0(t)} = -2+e^{-\frac{1}{2\gamma_\lambda}}+e^{-\frac{K^2}{2\gamma_\lambda}}$, $\alpha = \frac{1}{\sqrt{2}}$, and $\beta = \sqrt{2}$. For the case of $g_-(t)$, factor F is given by $F_{g_-(t)} = (3e^{-\frac{1}{2\gamma_\lambda}} - 4e^{-\frac{1}{8\gamma_\lambda}} + e^{-\frac{K^2}{2\gamma_\lambda}})$, $\alpha = \frac{\sqrt{2}}{3}$, and $\beta = \sqrt{2}$. For the case $g_+(t)$, $F_{g_+(t)} = (e^{-\frac{1}{2\gamma_\lambda}} - 4e^{-\frac{1}{8\gamma_\lambda}} + 3e^{-\frac{K^2}{2\gamma_\lambda}})$, $\alpha = \frac{\sqrt{2}}{3}$, and $\beta = \sqrt{2}$. The profile for Eq. (15), for $g_0(t)$, can be visualized in Fig. 4(a). It is possible to verify that as the maximum external asymmetry $g_{\max}$ is increased, the probability of the system reaching X_+ is also increased. This was to be expected from the deterministic simulations showed before in Fig. 2. We can also observe speed-dependent attractor selection as was previously predicted: higher rates γ_λ of passage through the critical region reduce the probability of reaching the branch of solutions (X_+) favored by the external asymmetry. Additionally, the differences between the probabilities calculated with constant and time-dependent asymmetry grow with γ_λ [see both Fig. 4(a) and the last expression in Eq. (15)], a result coherent with the deterministic solutions shown in Fig. 2.

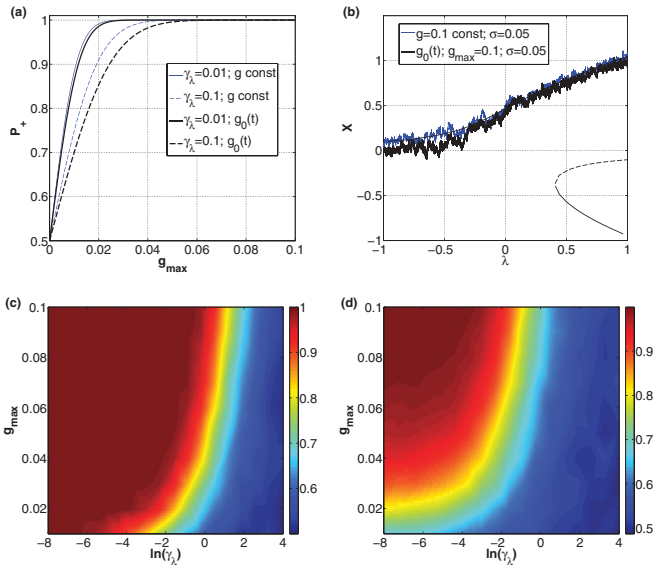

FIG. 4. (Color online) Branch selection probability dependence on asymmetry and sweeping speed. (a) Profile for probability P_+ of selection of X_+, under $g_0(t)$, determined by Eq. (15), for $\gamma_\lambda = 0.01$ and $\gamma_\lambda = 0.1$. Also shown are the curves obtained for P_+ with $g(t) = \mathrm{const}$ [calculated by the last expression in Eq. (15)]. For all curves, $\sigma = 0.05$. (b) Time series for $g(t) = \mathrm{const}$ and $g_0(t)$, with noise intensity $\sigma = 0.05$ and $\gamma_\lambda = 0.01$. (c) Effect of γ_λ and $g_{\max}$ on the fraction of trajectories ending up on X_+, determined numerically. The figure shows the result of fitting a surface to a 100×100 grid of points (γ_λ,$g_{\max}$), for noise intensity $\sigma = 0.05$. (d) Fraction of trajectories reaching X_+ for $\sigma = 0.2$.

One interesting aspect of the expressions derived for P_+ is the dependence on the $\frac{g_{\max}}{\sigma}$ ratio. Similar profiles are obtained if, for a raise in noise intensity σ, the maximum asymmetry allowed is also raised by the same amount. This ratio dependence is also a feature for the case of a constant asymmetry [8], and to an extent for the genetic circuit studied in [6]. A crucial aspect of Eq. (15) is the presence of a second term, $F_{g_-(t),g_0(t),g_+(t)}(\frac{\gamma_\lambda}{\pi})^{1/4}$. This contribution differs considerably from the original expression obtained with $g(t) = \mathrm{const}$ [see expression after the $\leqslant$ sign in Eq. (15)] [8]. This term is always smaller than $\beta(\frac{\pi}{\gamma_\lambda})^{\frac{1}{4}}$. It reflects the fact that although the probability density $P(X,t)$ drifts towards the upper branch more efficiently when γ_λ is smaller, the noise intensity and,

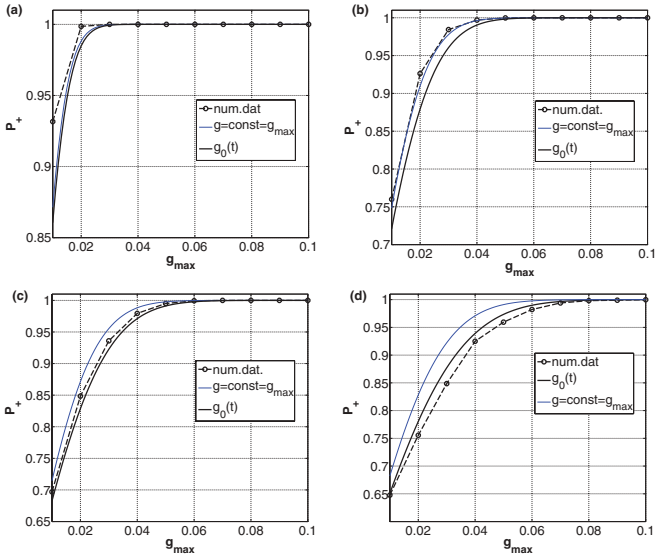

FIG. 5. (Color online) Numerical vs analytical branch selection probabilities. Each plot corresponds to a section of Fig. 4 for varying $g_{\max}$ and (a) $\gamma_\lambda = 0.01$, (b) $\gamma_\lambda = 0.1$, (c) $\gamma_\lambda = 0.2$, and (d) $\gamma_\lambda = 0.4$. For all figures, $\sigma = 0.05$. For the analytical curves, see also Eq. (15).

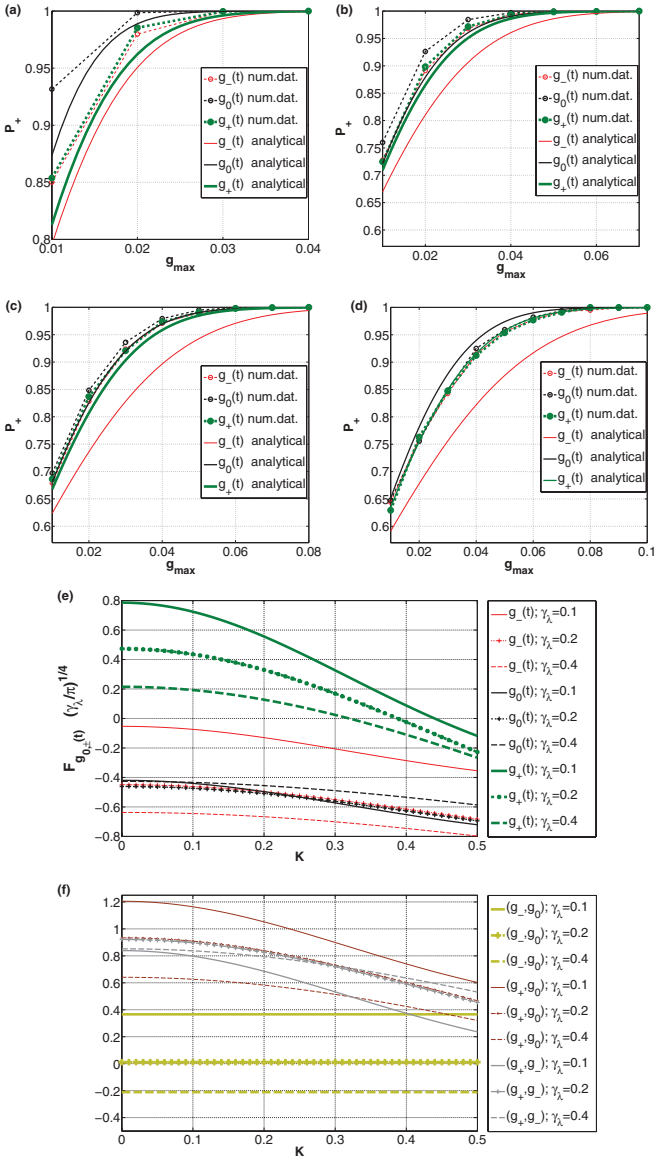

FIG. 6. (Color online) Probability dependence on reaching maximum asymmetries before, at, and after the critical region. The curves were obtained by plotting numerical results for $g_0(t)$, $g_-(t)$, and $g_+(t)$ and their respective analytical solutions [see Eq. (15)] with (a) $\gamma_\lambda = 0.01$, (b) $\gamma_\lambda = 0.1$, (c) $\gamma_\lambda = 0.2$, and (d) $\gamma_\lambda = 0.4$. (e) Term differentiating the computed probabilities with $g_0(t)$, $g_+(t)$, and $g_-(t)$ for several rates γ_λ [see Eq. (15)]. Although the relative magnitude of the curves resulting from $g_0(t)$ and $g_+(t)$ seems to not be compatible with the relative probabilities observed in (a)–(d), one should remember that in Eq. (15) the term that ultimately determines the magnitude of the probability is $\beta(\frac{\pi}{\gamma_\lambda})^{\frac{1}{4}}$, which is larger for the case of $g_0(t)$. (f) Pairwise difference between terms plotted in (e). For all cases, noise intensity $\sigma = 0.05$.

therefore, the spreading of the distribution is increased when sweeping speeds are low [see also Eqs. (9) and (13)].

To further understand the effect of different maximum asymmetries and sweeping speeds on the decision bias, extensive numerical experiments were performed for the cases when $g_0(t)$, $g_-(t)$, and $g_+(t)$ are applied to the system [see Figs. 4(c) and 4(d) for the case of $g_0(t)$]. Observing the color map of Fig. 4(c), one verifies that for $\ln(\gamma_\lambda) < 2$, the great majority of the $g_{\max}$'s induce selectivities above 60%. Selectivity or P_+ is equated with the probability of reaching the upper branch, i.e., the number of trajectories reaching X_+ from a batch of 5000. Raising the speed at which the system crosses the critical region increases symmetry between the distributions of the final attractors, as can be seen by the predominance of the blue region for larger values of $\ln(\gamma_\lambda)$. If we further raise the noise intensity, speed-dependent effects are still observed, but the region where a high probability of selecting X_+ is observed contracts towards lower values of γ_λ and higher values of $g_{\max}$ [see Fig. 4(d)]. In fact, there is a minimum $g_{\max}$ for which the lowest sweeping rates still generate selectivities above 50%. For higher intensity of fluctuations, branch to branch transitions are more common and therefore the assumptions behind the sweeping process and the derivation of Eq. (15) are no longer valid. Further treatment based on Kramers theory [17] is necessary and will complement the approach presented here for the bistable potential and, in [6], for the genetic switch. We should add that the features of the color map observed in Fig. 4(d) are also characteristic of those obtained with functions $g_\pm(t)$ (figure not shown).

Regarding the fit between the analytical expressions devised above and the numerical results obtained through extensive simulation, we observe that (see Fig. 5) for the case of the asymmetry profile $g_0(t)$, there is an interval of sweeping rates which includes $\gamma_\lambda = 0.2$ that generates the best fit [Fig. 5(c)]. Outside this region, the analytical expressions either underestimate [for small $\gamma'_\lambda s$; Figs. 5(a) and 5(b)] or overestimate [for large $\gamma'_\lambda s$; Fig. 5(d)] the probabilities P_+ determined numerically.

B. Effects of reaching the maximum asymmetry at, below, or beyond the critical point

Let us now observe the results presented in Fig. 6. The numerical curves indicate that $g_0(t)$ always generates higher

selectivities than the other cases [Figs. 6(a)–6(d)]. This is also predicted by the respective analytical results computed through Eq. (15). Although one could expect, by simply observing the numerically computed trajectories shown in Fig. 2, that $g_-(t)$ would generate higher P_+'s due to the fact that it induces a higher drift towards the upper branch (X_+) before $\lambda = 0$, $g_0(t)$ is, nevertheless, more efficient in dealing with the effects of noise. This stems from the fact that with respect to $g_-(t)$, $g_0(t)$ forces λ_i [Fig. 1(b)] to have higher values exactly when the fluctuations have a larger amplitude. Remember that in the vicinity of the critical region, fluctuations are amplified [18]. Regarding the effects of $g_+(t)$, although it generates paths closer to the unstable branch and therefore larger switching delays, it is still capable of giving rise to larger selectivities than those observed for $g_-(t)$. Once again, this probably comes from the interplay between the moment when the amplitude of the asymmetry is higher and the moment when the fluctuations are stronger. Further investigations are necessary to determine exactly the region where the maximum asymmetry should be reached with respect to the noise amplitude (along the lines of [18]). Regarding the speed-dependent effects observed in the numerical results presented in Figs. 6(a)–6(d), it is possible to verify that as the rate γ_λ is increased, the differences induced by each asymmetry function decrease. This is also valid for the differences between the theoretical probability results generated by $g_0(t)$ and $g_+(t)$ [observe Fig. 6(f), where the difference between the terms $F_{g_{0,\pm}(t)}(\frac{\gamma_\lambda}{\pi})^{\frac{1}{4}}$ distinguishing the probabilities induced with each asymmetry function is shown]. Regarding the analytical probability curves obtained with $g_-(t)$, these tend to be increasingly different from the other cases as the sweeping rate is raised [Fig. 6(f)].

Let us also compare the profiles obtained with Eq. (15) and those determined numerically. As was registered in Fig. 5, there is, for $g_0(t)$ and additionally for $g_+(t)$, a region of rates that generates the best fit. Regarding $g_-(t)$, the curves never really fit the numerical data. With increasing γ_λ, the $F_{g_-(t)}(\frac{\gamma_\lambda}{\pi})^{\frac{1}{4}}$ term pushes the argument on which the error function operates further to smaller values and, given the fact that erf(z) has a sigmoidal profile around 0, the differences with respect to the other cases are subsequently amplified.

Further analysis based on the long term behavior (see [16, 17]) of the solutions obtained when applying $g_-(t)$, $g_0(t)$, and $g_+(t)$ is necessary for the cases of large fluctuations where branch to branch transitions are present. Preliminary numerical simulations have shown that even with noise amplitudes of $\sigma = 0.5$, there is a significant region from $-3 < \ln(\gamma_\lambda) < -1$ and $0.05 < g_{\max} < 0.1$ where selectivity of the upper branch is larger than 0.65, therefore giving rise to the idea of an optimal γ_λ even for large fluctuations (figure not shown).

IV. OUTLOOK

In contrast to other aspects of nonequilibrium physics [25–27], dynamic bifurcations, as explored here and in [6], have not been systematically studied in systems biology despite involving fundamental aspects of cell fate decision, nor have they been adapted from canonical models to address biocircuits. It is of special interest in this context of cell fate decision because all genetic switches are asymmetric and stochastic and, hence, can be expected to demonstrate speed-dependent effects in attractor and phenotype selection. Devising a direct analytical link [9] between gene regulatory models [6] and the normal form characteristic of the bistable potential problem [8] will help us understand, in a consistent analytical framework, aspects of the speed-dependent cellular decision making mechanism [6], namely, the importance of both the sweeping speed through the critical region but also the relevance of reaching maximum external asymmetries before, at, and after the bifurcation points. It should reveal direct connections to the principal findings reported here for the bistable potential perturbed by $g_{0,\pm}(t)$: overall, the transient asymmetries are efficient selectors of a particular attractor if they reach their maximum values at an instant which pushes λ_i further away. This allows for the system to cope with the detrimental effects of large intensities of noise and retain memory of transient external perturbations.

Further studies in systems with more complicated dynamics such as the high-dimensional switch [7], or other paradigmatic circuits such as the repressilator with quorum sensing, where coexistence of point and dynamical attractors [12] is observed, should reveal further aspects of speed-dependent effects on cellular decision making. We also expect that investigations of the pattern selection process inherent to developmental biology [28] should find a crucial role for the theory explored in our work. Another avenue that seems promising for analytical understanding of speed-dependent effects is the recently developed theory of optimal paths for cell fate decision, based on the calculation of path integrals, in systems undergoing a bifurcation [29–31].

ACKNOWLEDGMENTS

N.R.N. acknowledges financial support from the EPSRC at CoMPLEX, UCL, provided during the research that led to the work presented here.

[1] S. Huang, G. Eichler, Yaneer Bar-Yam, and D. E. Ingber, Phys. Rev. Lett. **94**, 128701 (2005).

[2] T. Helikar, J. Konvalina, J. Heidel, and J. A. Rogers, Proc. Natl. Acad. Sci. USA **105**, 1913 (2008).

[3] S. L. Werner, D. Barken, and A. Hoffmann, Science **309**, 1857 (2005).

[4] L. O. Murphy, S. Smith, R. H. Chen, D. C. Fingar, and J. Blenis, Nature Cell. Biol. **4**, 556 (2002).

[5] S. Huang, Y. Guo, G. May, and T. Enver, Dev. Biol. **305**, 695 (2007).

[6] N. R. Nene, J. García-Ojalvo, and A. Zaikin, PLoS ONE **7**, e32779 (2012).

[7] N. R. Nene and A. Zaikin, PLoS ONE **7**, e40085 (2012).
[8] D. K. Kondepudi, F. Moss, and P. V. E. McClintock, Physica D **21**, 296 (1986).
[9] N. R. Nene (unpublished).
[10] T. Enver, M. Pera, C. Peterson, and P. W. Andrews, Stem Cell **4**, 387 (2009).
[11] V. Chickarmane, T. Enver, and C. Peterson, PLoS Comput. Biol. **5**, e1000268 (2009).
[12] E. Ullner, A. Zaikin, E. I. Volkov, and J. García-Ojalvo, Phys. Rev. Lett. **99**, 148103 (2007).
[13] B. Ermentrout, *Simulating, Analyzing, and Animating Dynamical Systems: A Guide to Xppaut for Researchers and Students (Software, Environments, Tools)* (North-Holland, Amsterdam, 2002), p. 290.
[14] T. Erneux, E. L. Reiss, L. J. Holden, and M. Georgiou, in *Dynamic Bifurcations*, Lecture Notes in Mathematics Vol. 1493, edited by E. Benoit (Springer-Verlag, Berlin, 1991), pp. 14–28.
[15] M. Behar and A. Hoffmann, Curr. Opin. Genet. Dev. **20**, 684 (2010).
[16] C. Nicolis and G. Nicolis, New J. Phys. **7**, 1 (2005).
[17] C. Nicolis and G. Nicolis, Phys. Rev. E **62**, 197 (2000).
[18] S. Grossmann and A. Mikhailov, Z. Phys. B **78**, 1 (1990).
[19] P. E. Kloeden and E. Platen, *Numerical Solution of Stochastic Differential Equations* (Springer, Berlin, 1999).
[20] C. W. Gardiner, *Handbook of Stochastic Methods for Physics, Chemistry and the Natural Sciences* (Springer, Berlin, 2004).
[21] D. K. Kondepudi and G. W. Nelson, Phys. Rev. Lett. **50**, 1023 (1983).
[22] F. Moss, D. K. Kondepudi, and P. V. E. McClintock, Phys. Lett. A **112**, 293 (1985).
[23] H. Crauel and F. Flandoli, J. Dyn. Diff. Equations **10**, 259 (1998).
[24] $\mathrm{erf}(z) = \frac{2}{\sqrt{\pi}} \int_0^z e^{-z'^2} dz'$.
[25] J. Berg, Phys. Rev. Lett. **100**, 188101 (2008).
[26] H. Ge and H. Qian, Phys. Rev. Lett. **103**, 148103 (2009).
[27] T. J. Kobayashi, Phys. Rev. Lett. **106**, 228101 (2011).
[28] M. Cohen, M. Georgiou, N. Stevenson, M. Miodownik, and B. Baum, Dev. Cell **19**, 78 (2010).
[29] J. Wang, K. Zhang, L. Xu, and E. Wang, Proc. Natl. Acad. Sci. USA **108**, 8257 (2011).
[30] N. Berglund and B. Gentz, *Noise-Induced Phenomena in Slow-Fast Dynamical Systems: A Sample-Paths Approach* (Springer, London, 2006).
[31] S. Wieczorek, P. Ashwin, C. M. Luke, and P. Cox, Proc. R. Soc. A **467**, 1243 (2011).